Available online at www.sciencedirect.com
SCIENCE DIRECT®
Journal of Molecular Spectroscopy 229 (2005) 145–149
Journal of MOLECULAR SPECTROSCOPY
www.elsevier.com/locate/jms

Note

Fourier transform infrared emission spectra of MnH and MnD

Iouli E. Gordon[a], Dominique R.T. Appadoo[b], Alireza Shayesteh[b], Kaley A. Walker[b], Peter F. Bernath[a,b,*]

[a] Department of Physics, University of Waterloo, Waterloo, Ont., Canada N2L 3G1
[b] Department of Chemistry, University of Waterloo, Waterloo, Ont., Canada N2L 3G1

Received 13 April 2004; in revised form 2 August 2004
Available online 25 September 2004

Abstract

Fourier transform infrared emission spectra of MnH and MnD were observed in the ground $X^7\Sigma^+$ electronic state. The vibration-rotation bands from $v = 1 \rightarrow 0$ to $v = 3 \rightarrow 2$ for MnH and from $v = 1 \rightarrow 0$ to $v = 4 \rightarrow 3$ for MnD were recorded at an instrumental resolution of 0.0085 cm^{-1}. Spectroscopic constants were determined for each vibrational level and equilibrium constants were found from a Dunham-type fit. The equilibrium vibrational constant (ω_e) for MnH was found to be 1546.84518(65) cm^{-1}, the equilibrium rotational constant (B_e) is 5.6856789(103) cm^{-1} and the eqilibrium bond distance (r_e) was determined to be 1.7308601(47) Å.

Keywords: MnH and MnD; Fourier transform spectrometer; Infrared spectrum; Equilibrium molecular constants

Manganese hydride is one of the most extensively studied high spin molecules. Between 1942 and 1957, Nevin and co-workers [1–6] recorded and rotationally analyzed the 0–0 and 0–1 bands of the $A^7\Pi$–$X^7\Sigma^+$ transition (near 568 and 624 nm) for MnH and MnD. The A–X 0–0 band was later revisited by Varberg et al. [7–9] using laser excitation spectroscopy. They have extended Nevin's rotational analysis to the lowest J values for every spin component and studied the nuclear hyperfine interaction.

Urban and Jones [10,11] observed an infrared spectrum of MnH and MnD using a diode laser spectrometer. They recorded vibrational bands $v = 1 \leftarrow 0$ to $v = 3 \leftarrow 2$, determined equilibrium constants for both molecules and carried out a combined isotopologue fit. Unfortunately semiconductor diode lasers cannot cover the whole spectral range of interest. As a result only relatively few infrared lines have been measured; for example only seven R-lines, that are all spin components of a single R(5) transition, were obtained for the fundamental band of MnH.

In this paper, we report new infrared emission spectra of MnH and MnD recorded with a Fourier transform spectrometer. The vibrational bands $v = 1 \rightarrow 0$ to $v = 3 \rightarrow 2$ for MnH and $v = 1 \rightarrow 0$ to $v = 4 \rightarrow 3$ for MnD were observed. Analyses of the new spectra have provided improved ground state molecular constants for MnH and MnD.

The same emission source that has proved to be very effective in providing spectra of other metal hydrides in our laboratory was used for MnH and MnD [12,13]. The infrared spectra of MnH/D were recorded between 800 and 1700 cm^{-1} at a resolution of 0.0085 cm^{-1}.

The recorded infrared emission spectrum of MnH/D contained vibration–rotation bands in the ground electronic $^7\Sigma^+$ state. The lines from $v = 1 \rightarrow 0$ to $v = 3 \rightarrow 2$ for MnH and the lines from $v = 1 \rightarrow 0$ to $v = 4 \rightarrow 3$ transitions for MnD were found and analyzed. An overview spectrum of MnD is shown on Fig. 1. To display the bands more clearly the baseline was corrected by eliminating blackbody emission profile using the Bruker OPUS program.

* Corresponding author. Fax: +1 519 746 0435.
E-mail address: bernath@uwaterloo.ca (P.F. Bernath).

0022-2852/$ - see front matter © 2004 Elsevier Inc. All rights reserved.
doi:10.1016/j.jms.2004.08.010

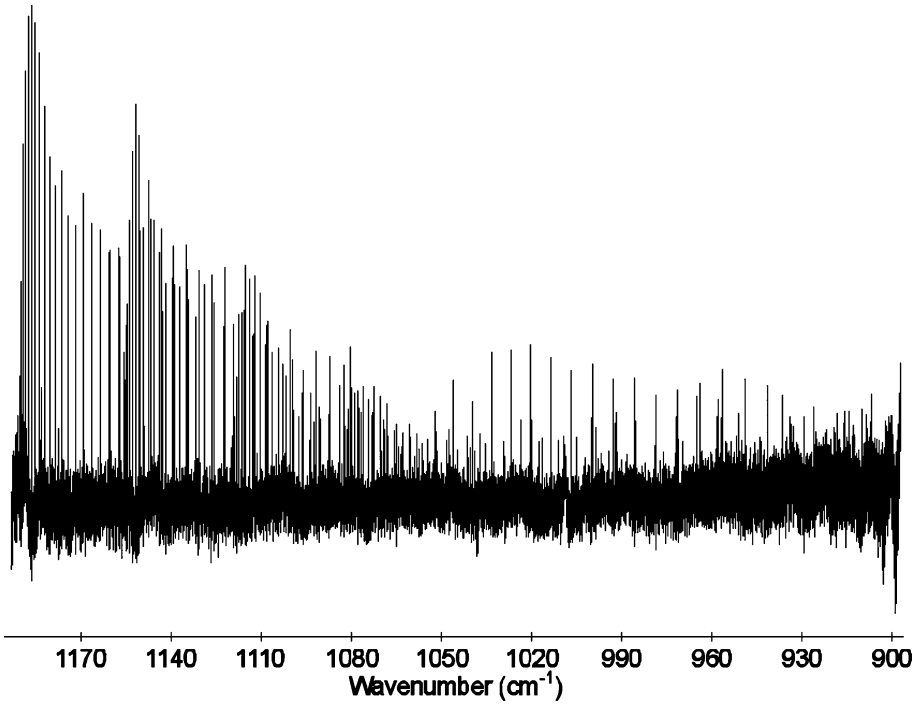

Fig. 1. An overview of the infrared emission spectrum of MnD after baseline correction.

The $X^7\Sigma^+$ state of MnH obeys Hund case (b) coupling so each rotational level (N) is split into seven spin components (for $N \geqslant 3$) labeled by J with $\mathbf{J} = \mathbf{N} + \mathbf{S}$, where $\mathbf{J}$ is the total angular momentum, $\mathbf{N}$ is rotational angular momentum and $\mathbf{S}$ is the total electron spin. Examples showing these seven spin components for R(5) and P(7) lines of the fundamental band of MnH are displayed in Fig. 2. The spacing between the spin components in the R branches decreases with increasing of N, causing transitions with $N > 20$ of fundamental band to be observed as single broad lines. This blending is observed to occur at lower N values as the vibrational quantum number increases. For the $v = 4 \rightarrow 3$ transition in MnD just completely blended R-lines were observed without any trace of corresponding P-lines. The intensities of the spin components of each rotational line both in the P- and R-branches increase from $J = N - 3$ to $J = N + 3$ as shown in Fig. 2 for R(5) and P(7) transitions of the fundamental band. These line intensities have the classic pattern given by coupling of two angular momenta such as $\mathbf{L}$ and $\mathbf{S}$ to give $\mathbf{J}$ for atoms [14]. Urban and Jones [10] observed deviations from this expected intensity pattern. In the present FT spectrum however this intensity pattern seems to be consistent throughout the spectrum. As an illustration, the lines in Fig. 2 were chosen to be the same as the ones shown in [10]. In our spectrum we were also able to observe a few satellite lines (transitions across spin components) at low N values.

The line positions were determined using the program WSpectra [15] written by M. Carleer. The MnH/D spec-

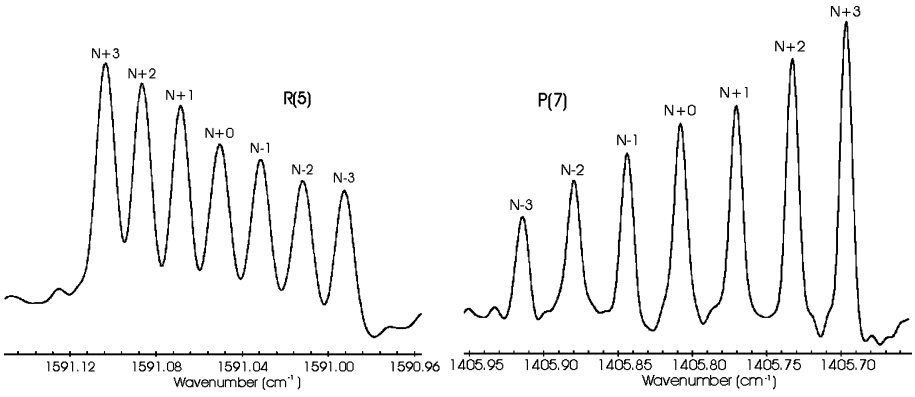

Fig. 2. Example of spin-splitting in MnH lines: R(5) and P(7) transitions of the fundamental band. The intensities of the spin components of each rotational line both in the P- and R-branches increase from $J = N - 3$ to $J = N + 3$. The spin components are labeled by J values.

Table 1
Equilibrium constants (in cm^{-1}) for MnH

Constant	This work	Ref. [10]
$Y_{1,0}$	1546.84518(65)	1546.8536(15)
$Y_{2,0}$	−27.59744(39)	−27.60280(91)
$Y_{3,0}$	−0.309037(67)	−0.30822(15)
$Y_{0,1}$	5.6856789(103)	5.685795(37)
$Y_{1,1}$	−0.1602038(70)	−0.160488(22)
$10^4\,Y_{2,1}$	−1.200(40)	0.405(91)
$10^4\,Y_{3,1}$	−3.0252(72)	−3.255(13)
$10^4\,Y_{0,2}$	−3.05384(58)	−3.0630(30)
$10^6\,Y_{1,2}$	1.397(22)	2.983(68)
$10^7\,Y_{2,2}$	−2.823(83)	−12.01(16)
$10^7\,Y_{3,2}$	−1.225(16)	—
$10^9\,Y_{0,3}$	9.4670(128)	8.68(60)
$10^9\,Y_{1,3}$	−1.551(48)	—
$10^{12}\,Y_{0,4}$	1.360(89)	—
$10^{13}\,Y_{1,4}$	9.16(39)	—
$10^2\gamma_{0,1}$	3.1749(35)	3.2055(83)
$10^4\gamma_{1,1}$	−7.698(54)	−8.32(13)
$10^5\gamma_{2,1}$	−4.100(101)	−3.40(33)
$10^6\gamma_{0,2}$	−6.763(53)	−7.54(21)
$10^7\gamma_{1,2}$	−2.554(98)	—
$10^3\lambda_{0,0}$	−3.758(92)	−3.35(12)[a]
$10^4\lambda_{1,0}$	−2.623(117)	—
$10^6\lambda_{0,1}$	−5.39(43)	−0.0195(27)[a]

Numbers in parentheses represent one standard deviation in units of the last digit.
[a] Calculated from values of $\varepsilon_{0,1}$ and $\varepsilon_{0,2}$ listed in [10].

tra were calibrated using the line positions of the previous diode laser infrared measurements [10,11]. The effect of blending at higher N values forced us to assign an experimental uncertainty ranging from 0.001 cm^{-1} for strong unblended lines to 0.003 cm^{-1} for completely blended lines (i.e., lines corresponding to seven spin components blended into one feature) for MnH and 0.001–0.005 cm^{-1} for MnD. Assignments were made for the fundamental band up to $N'' = 27$ for MnH, for the $v = 2 \rightarrow 1$ transition up to $N'' = 24$ and for the $v = 3 \rightarrow 2$ transition up to $N'' = 21$. The corresponding bands of MnD were assigned up to $N'' = 37$, $N'' = 36$, and $N'' = 33$, respectively. While the weak R-branch of the $v = 4 \rightarrow 3$ transition of MnD was followed up to $N'' = 29$. In total 874 MnH lines and 953 MnD lines were assigned.

SPFIT program [16] was used to carry out a Dunham-type fit to obtain equilibrium parameters for MnH and MnD using transitions up to $v = 3 \rightarrow 2$. The $v = 4 \rightarrow 3$ band of MnD was excluded because almost all of the observed lines were blended and the inclusion of these transitions led to an unsatisfactory fit. In this Dunham-type fit each parameter was assumed to have the usual vibrational dependence,

$$X_{ij} = X_{0j} + X_{1j}(v+\tfrac{1}{2}) + X_{2j}(v+\tfrac{1}{2})^2 + \cdots \quad (1)$$

indicated by first index for each parameter. The second index for each parameter indicates the order of the rotational dependence. The calculated equilibrium constants are provided in Table 1 for MnH and Table 2 for MnD. Then a fit was carried out with SPFIT to determine band constants and the results are presented in Table 3 for MnH and Table 4 for MnD. This time the $v = 4 \rightarrow 3$ band was included for MnD in the fit with spin–spin and spin–rotation constants fixed to the values calculated using equilibrium constants from Table 2.

No higher order parameters such as θ and γ_s were required to obtain a good fit. The diode laser lines of Ur-

Table 2
Equilibrium constants for MnD and Born–Oppenheimer breakdown parameters estimated using Eq. (2) (in cm^{-1})

Constant	This work	Ref. [11]	$\delta^{H}_{l,m}$	
$Y_{1,0}$	1104.65312(51)	1104.65225(93)	$\delta^{H}_{1,0}$	1.8268
$Y_{2,0}$	−14.22657(31)	−14.22656(54)	$\delta^{H}_{2,0}$	−0.6635
$Y_{3,0}$	−0.085848(52)	−0.085813(90)	$\delta^{H}_{3,0}$	0.14591
$Y_{0,1}$	2.8987214 (57)	2.898685(12)	$\delta^{H}_{0,1}$	0.009919
$Y_{1,1}$	−0.0581028(33)	−0.0580972(79)	$\delta^{H}_{1,1}$	−0.159557
$10^4\,Y_{2,1}$	−1.065(20)	−0.943(31)	$10^4\delta^{H}_{2,1}$	−5.8150
$10^4\,Y_{3,1}$	−0.4500(35)	−0.4784(44)	$10^4\delta^{H}_{3,1}$	1.1914
$10^4\,Y_{0,2}$	−0.796939(190)	−0.79584(54)	$10^4\delta^{H}_{0,2}$	0.03511
$10^6\,Y_{1,2}$	0.2543(41)	0.201(21)	$10^6\delta^{H}_{1,2}$	−0.048
$10^7\,Y_{2,2}$	−0.521(22)	−0.897(40)	$10^7\delta^{H}_{2,2}$	−2.239
$10^7\,Y_{3,2}$	−0.0870(38)	—	$10^7\delta^{H}_{3,2}$	0.6059
$10^9\,Y_{0,3}$	1.5713(197)	1.58(12)	$10^9\delta^{H}_{0,3}$	4.8464
$10^9\,Y_{1,3}$	−0.0957(30)	—	$10^9\delta^{H}_{1,3}$	1.0738
$10^2\gamma_{0,1}$	1.6234(30)	1.6388(67)		
$10^4\gamma_{1,1}$	−3.026(37)	−2.954(76)		
$10^5\gamma_{2,1}$	−0.831(99)	—		
$10^6\gamma_{0,2}$	−1.968(39)	−2.19(13)		
$10^3\lambda_{0,0}$	−1.823(55)	−1.44(21)[a]		
$10^4\lambda_{1,0}$	−1.17(11)	−1.33(19)[a]		

Numbers in parentheses represent one standard deviation in units of the last digit.
[a] Calculated from values of $\alpha_{0,1}$ and $\alpha_{1,1}$ listed in [11].

Table 3
Spectroscopic constants (in cm^{-1}) for the $X^7\Sigma^+$ ground state of MnH

Constant	$v=0$	0[a]	1	2	3
T_v	0	—	1490.644889(21)	2923.31542(34)	4296.15620(55)
B_v	5.6055050(96)	5.605746(71)	5.4441092(96)	5.2797006(106)	5.1104876(160)
$10^4 D_v$	3.04743(57)	3.0413(61)	3.04512(62)	3.05665(76)	3.08943(128)
$10^9 H_v$	8.639(131)	—	7.532(152)	5.926(196)	3.38(39)
$10^{12} L_v$	1.861(96)	—	2.473(122)	3.324(174)	5.12(39)
γ_v	0.031349(36)	0.030341(82)	0.030497(37)	0.029559(38)	0.028548(38)
$10^6 \gamma_{D_v}$	−6.902(58)	−11.0(12)	−7.159(64)	−7.399(71)	−7.681(80)
λ_v	−0.004020(92)	−0.00325(10)	−0.004230(92)	−0.004462(95)	−0.004778(103)
$10^6 \lambda_{D_v}$	−5.20(46)	0.0 (fixed)	−5.22(49)	−5.40(55)	−5.32(60)

Numbers in parentheses represent one standard deviation in units of the last digit.
[a] Constants for $v=0$ from [9].

Table 4
Spectroscopic constants (in cm^{-1}) for the $X^7\Sigma^+$ ground state of MnD

Constant	$v=0$	1	2	3	4
T_v	0	1075.920727(133)	2122.616176(206)	3139.57067(27)	4126.0780(25)
B_v	2.8696280(55)	2.8111700(52)	2.7520865(50)	2.6921167(51)	2.6310263(193)
$10^5 D_v$	7.95559(189)	7.94459(167)	7.94981(155)	7.97910(153)	8.0685(42)
$10^9 H_v$	1.5025(191)	1.4147(160)	1.3148(139)	1.2189(126)	1.295(27)
γ_v	0.0164400(181)	0.0161162(173)	0.0157850(166)	0.0154373(161)	0.014704[a]
$10^6 \gamma_{D_v}$	−2.418(34)	−2.410(31)	−2.396(28)	−2.403(25)	−1.97[a]
λ_v	−0.001637(58)	−0.001698(58)	−0.001855(58)	−0.002005(57)	−0.002350[a]

Numbers in parentheses represent one standard deviation in units of the last digit.
[a] Fixed to the values calculated from Table 2 using Eq. (1).

ban and Jones [10,11] were included in the fits; this was particularly helpful in the case of MnD since the diode laser spectrum was recorded at higher resolution than our Fourier transform measurements and some lines that were blended in our spectrum were resolved. The corresponding lines in our spectrum were given lower weight. Tables 1 and 2 list constants obtained by Urban and Jones [10,11] for comparison.

A few lines for certain low N values could not be fitted within the experimental uncertainty. This can be attributed to the internal hyperfine perturbations discussed by Varberg et al. [9]. Therefore, a larger uncertainty was assigned to those lines. This problem affected most of the observed satellite lines as well, which is particularly disadvantageous since these lines are very useful in determining better values for the spin–spin constants. Input and output files of SPFIT program are available on ScienceDirect.

The Born–Oppenheimer breakdown constants were estimated using Le Roy's formalism [17]:

$$Y_{l,m}^{\mathrm{MnD}} = \left\{ Y_{l,m}^{\mathrm{MnH}} + \frac{M_{\mathrm{D}} - M_{\mathrm{H}}}{M_{\mathrm{D}}} \delta_{l,m}^{\mathrm{H}} \right\} \left(\frac{\mu_{\mathrm{MnH}}}{\mu_{\mathrm{MnD}}} \right)^{(l+2m)/2}. \quad (2)$$

The estimated Born–Oppenheimer breakdown constants ($\delta_{l,m}^{\mathrm{H}}$) are given in Table 2.

The fit of the new and extensive dataset has provided an improved set of constants for the ground states of MnH and MnD, and allowed to determine higher order expansion constants in the Dunham-type fit. The equilibrium bond distance was determined to be 1.7308601(47) Å for MnH, based on the value of B_e calculated in the fit. Our spectroscopic constants for $v=0$ can also be compared with those of Varberg et al. [9] in Table 3. Varberg et al. [9] determined a value for θ and for γ_s (a cross-term between spin–rotation and spin–spin terms) that we find unnecessary. We find that the Born–Oppenheimer breakdown correction parameters ($\delta_{l,m}^{\mathrm{H}}$) are relatively large, as is usually the case for metal hydrides [12].

Acknowledgments

Financial support from the Natural Sciences and Engineering Research Council of Canada is gratefully acknowledged.

Appendix. Supplementary material

Supplementary data for this article are available on ScienceDirect (www.sciencedirect.com) and as part of the Ohio State University Molecular Spectroscopy Archives (http://msa.lib.ohio-state.edu/jmsa_hp.htm).

References

[1] T.E. Nevin, Proc. R. Irish Acad. 48 (1942) 1–45.
[2] T.E. Nevin, Proc. R. Irish Acad. 50 (1945) 123–137.
[3] T.E. Nevin, M. Conway, M. Cranley, Proc. Phys. Soc. A 65 (1952) 115–124.
[4] T.E. Nevin, P.G. Doyle, Proc. R. Irish Acad. 52 (1948) 35.
[5] T.E. Nevin, D.V. Stephens, Proc. R. Irish Acad. 55 (1953) 109.
[6] W. Hayes, P.D. McCarvill, T.E. Nevin, Proc. Phys. Soc. A 70 (1957) 904–905.
[7] T.D. Varberg, R.W. Field, A.J. Merer, J. Chem. Phys. 92 (1990) 7123–7127.
[8] T.D. Varberg, R.W. Field, A.J. Merer, J. Chem. Phys. 95 (1991) 1563–1576.
[9] T.D. Varberg, J.A. Gray, R.W. Field, A.J. Merer, J. Mol. Spectrosc. 156 (1992) 296–318.
[10] R.-D. Urban, H. Jones, Chem. Phys. Lett. 163 (1989) 34–40.
[11] R.-D. Urban, H. Jones, Chem. Phys. Lett. 178 (1991) 295–300.
[12] A. Shayesteh, D.R.T. Appadoo, I. Gordon, R.J. Le Roy, P.F. Bernath, J. Chem. Phys. 120 (2004) 10002–10008.
[13] A. Shayesteh, K. Walker, D.R.T. Appadoo, I. Gordon, P.F. Bernath, J. Mol. Struct. 695 (2004) 23–37.
[14] E.U. Condon, G. Shortley, The Theory of Atomic Spectra, Cambridge University Press, England, 1951.
[15] M. Carleer, Proc. SPIE 4168 (2001) 337.
[16] H.M. Pickett, J. Mol. Spectrosc. 148 (1991) 371–377.
[17] R.J. Le Roy, J. Mol. Spectrosc. 194 (1999) 189–196.